Journal of the Mechanics and Physics of Solids 70 (2014) 116–135

Contents lists available at ScienceDirect

Journal of the Mechanics and Physics of Solids

journal homepage: www.elsevier.com/locate/jmps

Some basic questions on mechanosensing in cell–substrate interaction

Shijie He [a], Yewang Su [a,b,*], Baohua Ji [a,**], Huajian Gao [c]

[a] Biomechanics and Biomaterials Laboratory, Department of Applied Mechanics, School of Aerospace Engineering, Beijing Institute of Technology, Beijing 100081, PR China
[b] Department of Civil and Environmental Engineering and Mechanical Engineering, Northwestern University, Evanston, IL 60208, USA
[c] School of Engineering, Brown University, Providence, RI 02912, USA

ARTICLE INFO

Article history:
Received 19 September 2013
Received in revised form
5 May 2014
Accepted 31 May 2014
Available online 10 June 2014

Keywords:
Cell–matrix interaction
Cell traction
Cell adhesion
Cell migration

ABSTRACT

Cells constantly probe their surrounding microenvironment by pushing and pulling on the extracellular matrix (ECM). While it is widely accepted that cell induced traction forces at the cell–matrix interface play essential roles in cell signaling, cell migration and tissue morphogenesis, a number of puzzling questions remain with respect to mechanosensing in cell–substrate interactions. Here we show that these open questions can be addressed by modeling the cell–substrate system as a pre-strained elastic disk attached to an elastic substrate via molecular bonds at the interface. Based on this model, we establish analytical and numerical solutions for the displacement and stress fields in both cell and substrate, as well as traction forces at the cell–substrate interface. We show that the cell traction generally increases with distance away from the cell center and that the traction-distance relationship changes from linear on soft substrates to exponential on stiff substrates. These results indicate that cell adhesion and migration behaviors can be regulated by cell shape and substrate stiffness. Our analysis also reveals that the cell traction increases linearly with substrate stiffness on soft substrates but then levels off to a constant value on stiff substrates. This biphasic behavior in the dependence of cell traction on substrate stiffness immediately sheds light on an existing debate on whether cells sense mechanical force or deformation when interacting with their surroundings. Finally, it is shown that the cell induced deformation field decays exponentially with distance away from the cell. The characteristic length of this decay is comparable to the cell size and provides a quantitative measure of how far cells feel into the ECM.

1. Introduction

Mechanosensing of adherent cells on elastic substrates is an issue of fundamental importance to the understanding of a range of phenomena in cell mechanics including cell adhesion, cell migration and cell differentiation (Lo et al., 2000; Discher et al., 2005; Peyton and Putnam, 2005; Yeung et al., 2005; Engler et al., 2006; Tee et al., 2011; Zhong and Ji, 2014). When cultured on a substrate, cells constantly probe, push and pull on the substrate via traction forces at the cell–substrate interface

* Corresponding author at: Biomechanics and Biomaterials Laboratory, Department of Applied Mechanics, School of Aerospace Engineering, Beijing Institute of Technology, Beijing 100081, PR China.
** Corresponding author.
E-mail addresses: yewangsu@gmail.com (Y. Su), bhji@bit.edu.cn (B. Ji).

http://dx.doi.org/10.1016/j.jmps.2014.05.016
0022-5096/

induced by the myosin driven contractility in the cytoskeleton (Harris et al., 1980). These forces drive cell migration and tissue morphogenesis, and maintain the intrinsic mechanical tone of tissues. In spite of intense interests and tremendous progresses over several decades, the precise distribution and regulation mechanisms of cell traction forces are still poorly understood, partly due to the complexity of cell behaviors and insufficient resolution of existing cell traction force microscopy techniques (Gardel et al., 2008; Ghassemi et al., 2012; Polio et al., 2012). Much further work is needed before a thorough understanding of the principles of cellular mechanosensing under both physiological and pathological conditions can be achieved.

It is known that cells interact with their substrates through focal adhesion complexes (FACs) which not only mechanically anchor the cells on substrates, but also play critical roles in mechanosensing and mechanotransduction (Bershadsky et al., 2003). Mechanical forces appear to play critical roles in the stability of FACs. For example, it has been shown that a small pulling force on cells by micropipette induces growth of FACs (Balaban et al., 2001; Riveline et al., 2001; Tan et al., 2003), but a large pulling force on cells due to substrate stretching induces cell reorientation (Kaunas et al., 2005; Jungbauer et al., 2008; Liu et al., 2008), and recent studies demonstrated that cell reorientation on substrates under cyclic stretch can be related to the stability of FACs (Kong et al., 2008a,b; Zhong et al., 2011; Chen et al., 2012; Qian et al., 2013). Further studies clarified that the stability of FACs exhibits a biphasic dependence on cell traction, with a stabilizing to disruptive transition as the traction is continuously increased (Kong et al., 2010; Zhong et al., 2011; Chen et al., 2012). The traction force dependent dynamics of stability of FACs can be crucial for mechanosensing of cells on substrates.

Substrate stiffness has also been recognized to play a key role in mechanosensing of cells. Experiments indicated that substrate stiffness has significant effects on the traction forces at the cell–substrate interface as well as the cell spreading area. On a substrate patterned with arrays of microposts, Fu and co-workers (Fu et al., 2010; Weng and Fu, 2011) observed that the cell traction force, cell spreading area, and total area of FACs all increase with the stiffness of the microposts, and the total traction force is linearly proportional to the cell spreading area. Tan et al. (2003) reported that the average force on the microposts increases with the cell spreading area. Ladoux and co-workers (Saez et al., 2005; Ghibaudo et al., 2008; Ladoux et al., 2010) found that the average force as well as the largest force on a micropost exhibit a biphasic dependence on the stiffness of the post, i.e., they increase linearly with the post stiffness when the latter is relatively soft, but then level off to a plateau value on sufficiently stiff posts (Fig. 1a). On a continuous substrate, it was reported that cell traction is proportional to the cell spreading area (Reinhart-King et al., 2005), the latter exhibiting a similar biphasic dependence on the substrate stiffness (Sen et al., 2009). However, in spite of the accumulating experimental evidence, the biphasic dependence of cell traction on substrate stiffness has not been satisfactorily explained. This lack of understanding has resulted in an on-going debate on whether cells sense force or deformation on an elastic substrate (Freyman et al., 2002; Tan et al., 2003; Saez et al., 2005).

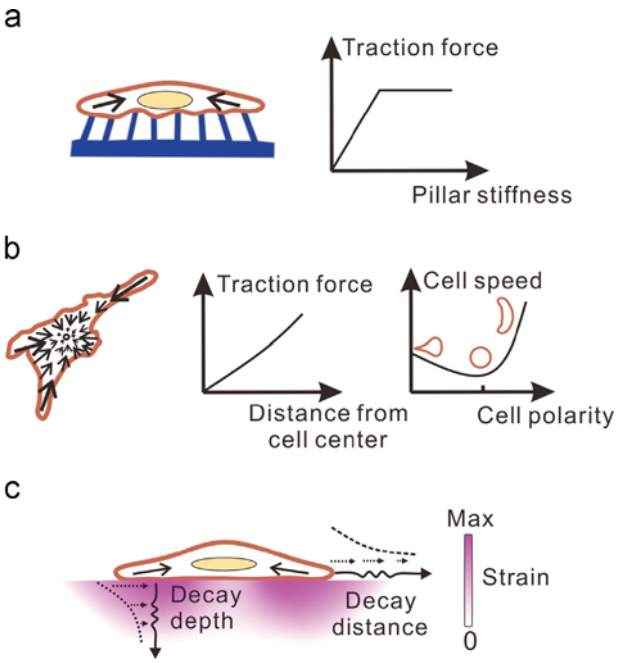

Fig. 1. Mechanosensing of cells on elastic substrates. (a) Cell exerts traction forces and deflects an array of elastomeric micro-posts on substrate. The cell traction exhibits a biphasic dependence on the stiffness of the micro-posts. (b) A traction–distance law in cellular mechanosensing: the larger the distance from the cell center, the higher the cell traction. The commonly observed polarized cell shape is expected to play a crucial role in tuning the distribution of traction force and controlling cell migration behaviors. (c) The cell induced deformation field in the substrate decays with depth or distance away from the cell, which defines the characteristic length of cellular mechanosensing.

Besides magnitude, the distribution of cell traction has also received considerable attention. Rape et al. (2011) conducted a systematic study on the dependence of cell traction on cell geometry and spreading area, and observed that the cell traction and the size of FACs are both proportional to the distance from the cell center (Fig. 1b). Gardel et al. (2008) and Dembo and Wang (1999) showed that the cell traction decreases with distance from the cell edge in migrating keratocytes and fibroblasts. Similar traction–distance relationship has been observed in cell colonies (Mertz et al., 2012) and cells cultured in 3D matrices (Legant et al., 2010). A general observation is that the cell traction force increases with distance from the cell center: the larger the distance, the higher the traction force. Surprisingly, so far there is relatively little discussion on the mechanisms underlying the observed force-distance relationship, which can have important implications on cell migration behaviors and the role of cell shape in regulating traction distribution.

While it is known that cells actively sense a substrate by actively pulling and pushing on it, the interesting question of how far and deep cells can feel into their surroundings still has not been satisfactorily addressed, despite the fundamental importance of this question in understanding the mechanosensing of cells. It has been shown that mesenchymal stem cells exhibit enhanced spreading on thin gels ($\sim$500 nm) than on thick ones (70 μm) (Engler et al., 2006); The strains induced by cell contraction are generally larger on thinner gels and decrease rapidly with increasing gel thickness. Studies also indicated that the displacements and strains on gel surfaces decay rapidly with distance away from the cell periphery (Sen et al., 2009) (Fig. 1c). However, literature estimates of the mechanosensing distance of cells vary from a couple of microns to several tens of microns, as a result of various attempts to associate the cellular mechanosensing distance to cell length (Butler et al., 2002), cell height (Engler et al., 2004), magnitude of surface displacements or size of focal adhesions (Sen et al., 2009). A quantitative understanding of how far and deep cells can feel into their surroundings and how the thickness of a substrate affects the mechanosensing distance of cells remains to be clarified.

A variety of theoretical models have been developed from different perspectives to interpret experimental observations. Nicolas and Safran (2006) developed a two-layered model of a single FAC interacting with an elastic substrate and showed that the FAC prefers to grow on a stiffer substrate. Chen and Gao (2006) adopted a generalized JKR model in analyzing the stability of cell adhesion under substrate stretching. Lemmon and Romer (2010) studied the distribution of cell traction by modeling cell as a network of stress fibers each represented as a linear elastic truss with a uniform tensional pre-strain; However, these authors made a strong assumption that the contractile force in a stress fiber is proportional to its length, which is unfortunately applicable only on a sufficiently soft matrix (Zhong et al., 2012). Deshpande et al. (Deshpande et al., 2008; Pathak et al., 2008) developed a FEM based biomechanical model that takes into account the dynamic reorganization of cytoskeleton and FACs in modeling cell contractility and cell–matrix interaction; They showed that the FACs tend to aggregate at cell periphery. Edwards and Schwarz (2011) developed a simple and elegant model to calculate the traction force of a cell layer on microposted substrate by treating the microposts as elastic springs, with results indicating that cell traction prefers to localize at the periphery of the layer, in consistency with the experimental results of Mertz et al. (2012).

While the above studies represent tremendous progresses in understanding cell–matrix interactions, a few open questions remain to be clarified:

1) Why is cell traction distributed in a distance-dependent manner? What implications does this have on cell migration behaviors? Can cell migration be controlled by regulating the distribution of cell traction?
2) What is the mechanism by which substrate stiffness influences the magnitude and distribution of cell traction?
3) Do cells sense mechanical deformation or force on a substrate?
4) How far and deep can cells feel into a substrate?

In view of these open questions and experimental observations that have resulted in often fragmented and sometimes confusing conclusions on different facets of the problem, here we propose an alternative approach by modeling the cell–substrate system as a pre-strained elastic disk attached to an elastic substrate via adhesion molecules at the cell–substrate interface. We will show that this model has all the essential features of a contracting cell body on a substrate, and is also simple enough to allow analytical treatment. We first relate the deformation field in the substrate to traction forces at the cell–matrix interface based on the Boussinesq–Cerruti solution. A set of governing equations and boundary conditions are then obtained by linking the deformation of cell and substrate via molecular bonds at the cell–substrate interface. We consider the effects of substrate stiffness, substrate thickness, adhesion molecules and cell spreading area on the cell traction as well as the deformation fields in the cell and substrate. To our best knowledge, this is the first analytical model capable of integrating cell contractility with elastic deformation of cell, substrate as well as adhesion molecules along the interface. We will show that this model can explain essentially all experimental observations with respect to mechanosensing of cells on substrate, and therefore has the potential to provide a quantitative understanding of the mechanisms that regulate cell interactions with elastic substrates, including the magnitude and distribution of cell traction forces, as well as their implications on cell adhesion and migration behaviors.

2. Contracting disk model and analytical solutions

Due to the intrinsic contractility of cytoskeleton, cells have been frequently modeled as an elastic body with pre-strain ε_0 (Deshpande et al., 2008; Chen and Gao, 2010; Edwards and Schwarz, 2011; Friedrich and Safran, 2012). For cells adhering on

an elastic substrate, cell contraction induces deformation in the substrate (Harris et al., 1980) and traction forces (shear force) at the cell–substrate interface. Experimental observations have shown that the pre-strain of cells is usually around $\varepsilon_0 = 0.1$ under physiological conditions (Deguchi et al., 2006; Lu et al., 2008; Zhong et al., 2011).

Note that force-dipoles can also be used to model the intrinsic contractility of cells, as done by Safran and coworkers in studying the cell–substrate interactions (Schwarz and Safran, 2002; Bischofs et al., 2004; Friedrich and Safran, 2012) and cell alignment on substrates under cyclic stretching (De et al., 2007; De and Safran, 2008; De et al., 2008). In principle, a pre-strain is equivalent to a continuous distribution of infinitesimal force dipoles. In the present work, we will show that it is more convenient to model cell contraction as a pre-strain in dealing with deformation and distribution of adhesion molecules at the cell–matrix interface.

To enable a model as simple as possible without losing the essential physics of the problem, we treat an adherent cell as a pre-strained elastic disk with the following two-dimensional plane stress constitutive equation

$$\sigma_{ij} = \frac{E_c}{1+\nu_c}\left(\varepsilon_{ij} + \frac{\nu_c}{1-\nu_c}\varepsilon_{kk}\delta_{ij}\right) + \frac{E_c}{1-\nu_c}\varepsilon_0\delta_{ij}, \tag{1}$$

where E_c is Young's modulus, ν_c Poisson's ratio of the cell and $i,j = 1,\ 2$. The second term in the above equation accounts for the cytoskeletal contractility.

Fig. 2 shows schematically a cell adhering on a substrate via adhesion molecules at the cell–substrate interface. The cell has radius R, while the interfacial adhesion molecules have spring constant k_b and areal number density ρ. Here we consider two different types of elastic substrates: a continuous substrate and a micropost-patterned substrate.

From deformation compatibility, the radial elongation of a molecular bond at the interface is

$$\Delta_r(r) = u_s(r) - u_c(r) \tag{2}$$

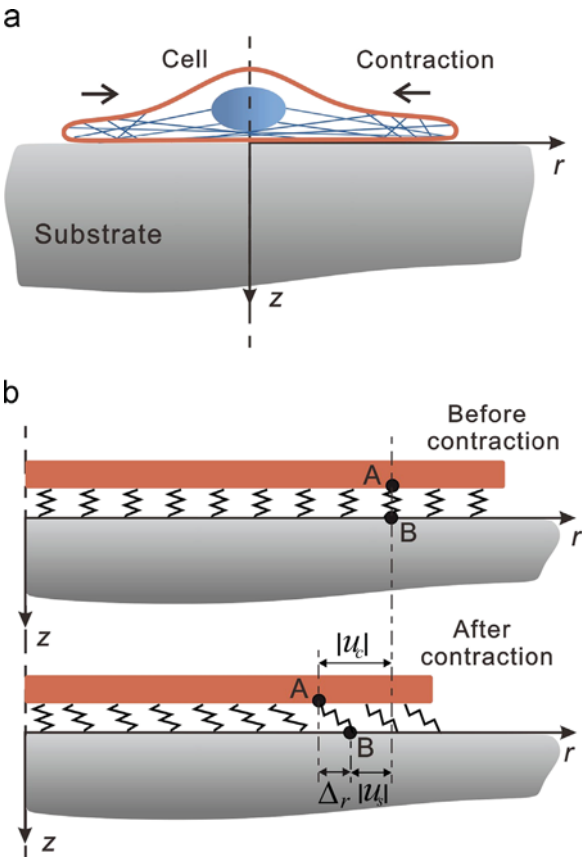

Fig. 2. Contracting disk model of cell–matrix interaction. (a) Schematic of a cell adhering and pulling on an elastic substrate due to the intrinsic contractility of cell. (b) The cell is modeled as an elastic contracting disk which is anchored on the substrate via molecular bonds (treated as elastic springs) at the cell–substrate interface. Before cell contraction, there is no elastic deformation in the system. Cell contraction induces displacements in the cell and substrate, denoted as u_c and u_s respectively, as well as elongation of molecular bonds $\Delta_r = u_s - u_c$.

where $u_c(r)$ and $u_s(r)$ denote radial displacements of the cell and substrate, respectively, as shown in Fig. 2. The cell traction $\tau_c(r)$ at the interface can be related to $\Delta_r(r)$ as

$$\tau_c(r) = \rho k_b \Delta_r(r) \tag{3}$$

where ρk_b is the areal stiffness of the interfacial bonds.

From the axisymmetry of the model, the equilibrium equation of the cell disk is

$$\frac{d^2u_c(r)}{dr^2} + \frac{1}{r}\frac{du_c(r)}{dr} - \frac{1}{r^2}u_c(r) + \frac{1}{E_c^* h_c}\tau_c(r) = 0, \tag{4}$$

subject to boundary conditions

$$\begin{cases} u_c(r) = 0 & r = 0 \\ \sigma_r = E_c^*\left(\frac{du_c(r)}{dr} + \nu_c\frac{u_c(r)}{r}\right) + \frac{E_c}{1-\nu_c}\varepsilon_0 = 0 & r = R, \end{cases} \tag{5}$$

where h_c is the height of the cell and E_c^* represents $\frac{E_c}{1-\nu_c^2}$. Because the bond elongation Δ_r is a function of substrate displacement u_s, next we need to relate the substrate deformation to the interfacial traction.

2.1. Cell on a semi-infinite substrate

2.1.1. Surface displacement of a semi-infinite substrate

Our first step is to relate the substrate surface displacement u_s to the interfacial traction (Fig. 3)

$$\tau_s = \tau_c. \tag{6}$$

Without loss of generality, we consider displacement at point C $(r, 0)$ induced by an infinitesimal traction force $\tau_s dA$ at an arbitrary point $D(r', \theta)$ inside the cell domain S at the interface. The coordinates of C can be expressed in terms of a local Cartesian coordinate system centered at D as (Fig. 3)

$$\begin{cases} x = r' - r\cos\theta \\ y = -r\sin\theta \end{cases} \tag{7}$$

According to the well-known Boussinesq–Cerruti solution (see Eq. (S1.1) in Supporting information), the surface displacements $(z = 0)$ at C induced by a force $\tau_s dA$ at D are (Johnson, 1987)

$$\begin{cases} du = \frac{(1+\nu_s)}{\pi E_s\sqrt{x^2+y^2}}\left(1 - \nu_s\frac{y^2}{x^2+y^2}\right)\tau_s dA \\ dv = \frac{(1+\nu_s)\nu_s xy}{\pi E_s (x^2+y^2)^{\frac{3}{2}}}\tau_s dA \end{cases} \tag{8}$$

where E_s and ν_s denote Young's modulus and Poisson's ratio of the substrate, respectively. The radial displacement at C is

$$d\tilde{u}_s(r, r') = -du\cos\theta - dv\sin\theta. \tag{9}$$

Substituting (7) and (8) into (9) leads to

$$d\tilde{u}_s(r, r') = \frac{\tau_s dA}{2\pi G_s}\left(\frac{\nu_s r r'\sin^2\theta}{(r'^2 - 2rr'\cos\theta + r^2)^{\frac{3}{2}}} - \frac{\cos\theta}{\sqrt{r'^2 - 2rr'\cos\theta + r^2}}\right) \tag{10}$$

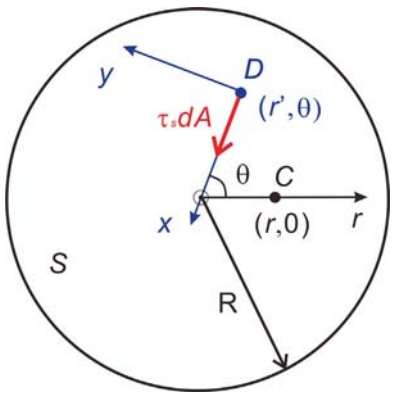

Fig. 3. Coordinates used to calculate displacement at point C $(r, 0)$ on the substrate surface using the Boussinesq–Cerruti solution of a point force of magnitude $\tau_s dA$ applied at another point D (r', θ) in the cell domain S on the substrate surface.

where $G_s = E_s/(2(1+\nu_s))$ is the shear modulus of the substrate. The radial displacement $u_s(r)$ induced by contraction of the whole cell can be obtained by integrating $d\tilde{u}_s(r,r')$ over the cell domain S as

$$u_s(r) = \int_S d\tilde{u}_s(r,r') \tag{11}$$

Substituting (10) into (11) and performing area integration with $dA = r'dr'd\theta$ yield

$$u_s(r) = \frac{2}{\pi E_s^*}\int_0^R f\left(\frac{r'}{r}\right)\tau_c(r')dr' \tag{12}$$

where $E_s^* = E_s/(1-\nu_s^2)$, and

$$f\left(\frac{r'}{r}\right) = (1+r'/r)\text{EllipticE}\left(\frac{2\sqrt{r'/r}}{1+r'/r}\right) - \frac{((r'/r)^2+1)}{1+r'/r}\text{EllipticK}\left(\frac{2\sqrt{r'/r}}{1+r'/r}\right) \tag{13}$$

where $\text{EllipticE}(x) = \int_0^1 \frac{\sqrt{1-x^2t^2}}{\sqrt{1-t^2}}dt$ and $\text{EllipticK}(x) = \int_0^1 \frac{1}{\sqrt{(1-t^2)(1-x^2t^2)}}dt$.

2.1.2. Governing equation of the cell–matrix system

According to (2) and (3), the shear traction along the cell–matrix interface can be expressed in terms of cell and substrate deformation as

$$\tau_c(r) = \rho k_b(u_s(r) - u_c(r)). \tag{14}$$

Substituting (12) into (14), and the resulting equation into (4), we obtain the governing equation of the system in terms of cell displacement $u_c(r)$ as,

$$\frac{d^2u_c(r)}{dr^2} + \frac{1}{r}\frac{du_c(r)}{dr} - \left(\frac{1}{r^2} + \frac{\rho k_b}{E_c^* h_c}\right)u_c(r) - \frac{2\rho k_b}{\pi E_s^*}\int_0^R f\left(\frac{r'}{r}\right)\left(\frac{d^2u_c(r')}{dr'^2} + \frac{1}{r'}\frac{du_c(r')}{dr'} - \frac{1}{r'^2}u_c(r')\right)dr' = 0 \tag{15}$$

For convenience, we introduce normalized variables $\bar{r} = r/R$, $\bar{r}' = r'/R$, $\bar{u}_c(\bar{r}) = u_c(r)/R$, and rewrite (15) and the associated boundary conditions in dimensionless form as

$$\frac{d^2\bar{u}_c(\bar{r})}{d\bar{r}^2} + \frac{1}{\bar{r}}\frac{d\bar{u}_c(\bar{r})}{d\bar{r}} - \left(\frac{1}{\bar{r}^2} + \frac{\rho k_b R^2}{E_c^* h_c}\right)\bar{u}_c(\bar{r}) - \frac{2\rho k_b R}{\pi E_s^*}\int_0^1 f\left(\frac{\bar{r}'}{\bar{r}}\right)\left[\frac{d^2\bar{u}_c(\bar{r}')}{d\bar{r}'^2} + \frac{1}{\bar{r}'}\frac{d\bar{u}_c(\bar{r}')}{d\bar{r}'} - \frac{1}{\bar{r}'^2}\bar{u}_c(\bar{r}')\right]d\bar{r}' = 0 \tag{16}$$

$$\begin{cases} \bar{u}_c(\bar{r}) = 0 & \bar{r} = 0 \\ E_c^*\left(\frac{d\bar{u}_c(\bar{r})}{d\bar{r}} + \nu_c\frac{\bar{u}_c(\bar{r})}{\bar{r}}\right) + \frac{E_c}{1-\nu_c}\varepsilon_0 = 0 & \bar{r} = 1 \end{cases} \tag{17}$$

2.1.3. Solution to the governing equation

Eq. (16) indicates that the solution is governed by two dimensionless parameters $a = 2\rho k_b R/(\pi E_s^*)$ and $b = \rho k_b R^2/(E_c^* h_c)$. It can be shown that $a < 1$ for most practical situations. Therefore, we adopt a perturbation approach by expanding $\bar{u}_c(\bar{r})$ as

$$\bar{u}_c(\bar{r}) = \sum_{m=0}^{\infty} a^m \bar{u}_{c(m)}(\bar{r}). \tag{18}$$

Substituting (18) into (16) and (17) allows us to obtain governing equations and boundary conditions to different orders in a^m. The zeroth-order equation and associated boundary conditions ($m = 0$), corresponding to the case of cell on a rigid substrate, are

$$\frac{d^2\bar{u}_{c(0)}(\bar{r})}{d\bar{r}^2} + \frac{1}{\bar{r}}\frac{d\bar{u}_{c(0)}(\bar{r})}{d\bar{r}} - \left(\frac{1}{\bar{r}^2} + b\right)\bar{u}_{c(0)}(\bar{r}) = 0 \tag{19}$$

$$\begin{cases} \bar{u}_{c(0)}(\bar{r}) = 0 & \bar{r} = 0 \\ E_c^*\left(\frac{d\bar{u}_{c(0)}(\bar{r})}{d\bar{r}} + \nu_c\frac{\bar{u}_{c(0)}(\bar{r})}{\bar{r}}\right) + \frac{E_c}{1-\nu_c}\varepsilon_0 = 0 & \bar{r} = 1 \end{cases} \tag{20}$$

The higher-order ($m = 1, 2, \cdots$) governing equations and the associated boundary conditions are

$$\frac{d^2\bar{u}_{c(m)}(\bar{r})}{d\bar{r}^2} + \frac{1}{\bar{r}}\frac{d\bar{u}_{c(m)}(\bar{r})}{d\bar{r}} - \left(\frac{1}{\bar{r}^2} + b\right)\bar{u}_{c(m)}(\bar{r}) - F_m(\bar{r}) = 0 \tag{21}$$

$$\begin{cases} \overline{u}_{c(m)}(\overline{r})=0 & \overline{r}=0 \\ E_c^*\left(\frac{d\overline{u}_{c(m)}(\overline{r})}{d\overline{r}}+\nu_c\frac{\overline{u}_{c(m)}(\overline{r})}{\overline{r}}\right)=0 & \overline{r}=1 \end{cases} \tag{22}$$

where

$$F_{(m)}(\overline{r})=\int_0^1 f\left(\frac{\overline{r}'}{\overline{r}}\right)\left[\frac{d^2\overline{u}_{c(m-1)}(\overline{r}')}{d\overline{r}'^2}+\frac{1}{\overline{r}'}\frac{d\overline{u}_{c(m-1)}(\overline{r}')}{d\overline{r}'}-\frac{1}{\overline{r}'^2}\overline{u}_{c(m-1)}(\overline{r}')\right]d\overline{r}' \tag{23}$$

The solution to zeroth-order equation in (19) is

$$\overline{u}_{c(0)}(\overline{r})=C_{1(0)}\mathrm{BesselI}(1,\sqrt{b}\overline{r})+C_{2(0)}\mathrm{BesselK}(1,\sqrt{b}\overline{r}) \tag{24}$$

where the coefficients $C_{1(0)}$ and $C_{2(0)}$ are determined from boundary conditions (20) as

$$\begin{cases} C_{1(0)}=\frac{(1+\nu_c)e_0}{(1-\nu_c)\mathrm{BesselI}(1,\sqrt{b})-\sqrt{b}\mathrm{BesselI}(0,\sqrt{b})} \\ C_{2(0)}=0 \end{cases} \tag{25}$$

From Eq. (21), the higher order perturbation solutions are obtained as

$$\begin{aligned} \overline{u}_{c(m)}(\overline{r})=&C_{1(m)}\mathrm{BesselI}(1,\sqrt{b}\overline{r})+C_{2(m)}\mathrm{BesselK}(1,\sqrt{b}\overline{r}) \\ &+\mathrm{BesselI}(1,\sqrt{b}\overline{r})\int_0^{\overline{r}}\mathrm{BesselK}(1,\sqrt{b}\overline{r})F_m(\overline{r})\overline{r}d\overline{r} \\ &-\mathrm{BesselK}(1,\sqrt{b}\overline{r})\int_0^{\overline{r}}\mathrm{BesselI}(1,\sqrt{b}\overline{r})F_m(\overline{r})\overline{r}d\overline{r} \end{aligned} \tag{26}$$

where $C_{1(m)}$ and $C_{2(m)}$ are coefficients determined from the boundary conditions (22) as

$$\begin{cases} C_{1(m)}=\chi\int_0^1\mathrm{BesselI}(1,\sqrt{b}\overline{r})F_m(\overline{r})\overline{r}d\overline{r}-\int_0^1\mathrm{BesselK}(1,\sqrt{b}\overline{r})F_m(\overline{r})\overline{r}d\overline{r} \\ C_{2(m)}=0 \end{cases} \tag{27}$$

where

$$\chi=\frac{(1-\nu_c)\mathrm{BesselK}(1,\sqrt{b})+\sqrt{b}\mathrm{BesselK}(0,\sqrt{b})}{(1-\nu_c)\mathrm{BesselI}(1,\sqrt{b})-\sqrt{b}\mathrm{BesselI}(0,\sqrt{b})} \tag{28}$$

Substituting (24) and (26) into (18) yields the final perturbation solution to the cell displacement. According to Eq. (4), the dimensionless cell traction $\overline{\tau}_c(\overline{r})=\tau_c(r)/E_c^*$ can be obtained from

$$\overline{\tau}_c(\overline{r})=-\frac{h_c}{R}\left(\frac{d^2\overline{u}_c(\overline{r})}{d\overline{r}^2}+\frac{1}{\overline{r}}\frac{d\overline{u}_c(\overline{r})}{d\overline{r}}-\frac{1}{\overline{r}^2}\overline{u}_c(\overline{r})\right). \tag{29}$$

In particular, the zeroth-order solution is found to be

$$\overline{\tau}_{c(0)}(\overline{r})=-\frac{h_c b}{R}C_{1(0)}\mathrm{BesselI}(1,\sqrt{b}\overline{r}) \tag{30}$$

The displacement and stress fields in the substrate can be calculated using Eqs. (S1.5) and (S1.6) in Supporting information S1. It is found that our perturbation solution converges at the second order. Therefore, only the zeroth, first and second order terms of Eq. (18) are included in our calculations.

2.2. Cell on a substrate of finite thickness

In the previous section, we have calculated the deformation of cell and substrate as well as interfacial traction on a semi-infinite substrate. In this subsection, we consider the same problem for cells on a substrate of finite thickness H.

According to Eqs. (S1.5) and (S1.6) in Supporting information S1, the displacements and stresses in a semi-infinite substrate decay exponentially with depth. We find that the substrate displacements can be approximately expressed as (Vlasov and Leonten, 1966)

$$u'_s(r,z)=u_s(r)h(z),\quad w'_s(r,z)=0 \tag{31}$$

where $u'_s(r,z)$ and $w'_s(r,z)$ are the radial and vertical displacements in the substrate, respectively, $u_s(r)$ being the radial displacement at the substrate surface and $h(z)$ decaying as

$$h(z)=\frac{\sinh\left[\alpha(H-z)/R\right]}{\sinh(\alpha H/R)} \tag{32}$$

For large H, $h(z)$ is an exponentially decaying function, consistent with the analytical and FEM based numerical solutions for a semi-infinite substrate. For small H, $h(z)$ becomes an approximately linear function, consistent with FEM simulations (see Fig. S1a in Supporting information). The parameter $\alpha\approx 4$ is a constant independent of the substrate stiffness and can be

calculated by considering the solution of a semi-infinite substrate (see Fig. S1b). Here assuming $w'_s(r,z)=0$ (Vlasov and Leonten, 1966) implies that the vertical displacements do not have significant effect on the in-plane deformation of cell and substrate, nor on the traction between them, when the thickness of the substrate is comparatively small. This assumption will be justified by a comparison with FEM simulations in the discussion of results.

Using a variational method (Supporting information S2), the governing equation of the substrate is obtained as

$$\begin{cases} E_s^1 c\frac{d^2u_{s1}}{dr^2}+\frac{E_s^1 c}{r}\frac{du_{s1}}{dr}-(G_s d+\frac{E_s^1 c}{r^2})u_{s1}-\tau_c=0, & 0\le r\le R \\ E_s^1 c\frac{d^2u_{s2}}{dr^2}+\frac{E_s^1 c}{r}\frac{du_{s2}}{dr}-(G_s d+\frac{E_s^1 c}{r^2})u_{s2}=0, & R<r<\infty \end{cases} \tag{33}$$

where $E_s^1=\frac{E_s(1-\nu_s)}{(1+\nu_s)(1-2\nu_s)}$, $c=\int_0^H h^2dz$, and $d=\int_0^H(\frac{dh}{dz})^2dz$.

Considering Eqs. (4), (33) and (14) leads

$$\begin{cases} \frac{d^2\overline{u}_c}{d\overline{r}^2}+\frac{1}{\overline{r}}\frac{d\overline{u}_c}{d\overline{r}}-\left(\frac{1}{\overline{r}^2}+b\right)\overline{u}_c+b\overline{u}_{s1}=0 \\ \frac{d^2\overline{u}_{s1}}{d\overline{r}^2}+\frac{1}{\overline{r}}\frac{d\overline{u}_{s1}}{d\overline{r}}-\left(\frac{1}{\overline{r}^2}+e+f\right)\overline{u}_{s1}+f\overline{u}_c=0 \\ \frac{d^2\overline{u}_{s2}}{d\overline{r}^2}+\frac{1}{\overline{r}}\frac{d\overline{u}_{s2}}{d\overline{r}}-\left(\frac{1}{\overline{r}^2}+e\right)\overline{u}_{s2}=0 \end{cases} \tag{34}$$

where $b=\frac{\rho k_b R^2}{E_s^* h_c}$, $e=\frac{G_s dR^2}{E_s^1 c}$ and $f=\frac{\rho k_b R^2}{E_s^1 c}$.

The cell displacement $\overline{u}_c$ should satisfy the boundary condition Eq. (17). The substrate displacement $\overline{u}_{s1}$ $(0\le\overline{r}\le 1)$ should satisfy $\overline{u}_{s1}=0$ at $\overline{r}=0$, and $\overline{u}_{s2}$ $(1\le\overline{r}<\infty)$ should satisfy $\overline{u}_{s2}=0$ at $\overline{r}=\infty$, and the displacement and normal stress of substrate should be continuous at the cell edge $\overline{r}=1$. Thus we obtain

$$\begin{cases} \overline{u}_c=0 & \overline{r}=0 \\ \frac{d\overline{u}_c}{d\overline{r}}+\nu_c\frac{\overline{u}_c}{\overline{r}}=-(1+\nu_c)\varepsilon_0 & \overline{r}=1 \\ \overline{u}_{s1}=0 & \overline{r}=0 \\ \overline{u}_{s1}=\overline{u}_{s2} & \overline{r}=1 \\ \frac{d\overline{u}_{s1}}{d\overline{r}}=\frac{d\overline{u}_{s2}}{d\overline{r}} & \overline{r}=1 \\ \overline{u}_{s2}=0 & \overline{r}=\infty \end{cases} \tag{35}$$

Solving (34) we obtain

$$\begin{cases} \overline{u}_c=C_1\mathrm{CBessell}(1,A\overline{r})+C_2D\mathrm{Bessell}(1,B\overline{r})+C_3\mathrm{CBesselK}(1,A\overline{r})+C_4D\mathrm{BesselK}(1,B\overline{r}) \\ \overline{u}_{s1}=2f[C_1\mathrm{Bessell}(1,A\overline{r})+C_2\mathrm{Bessell}(1,B\overline{r})+C_3\mathrm{BesselK}(1,B\overline{r})+C_4\mathrm{BesselK}(1,A\overline{r})] \\ \overline{u}_{s2}=C_5\mathrm{Bessell}(1,\sqrt{e}\overline{r})+C_6\mathrm{BesselK}(1,\sqrt{e}\overline{r}) \end{cases} \tag{36}$$

where

$$\begin{cases} A=\sqrt{\left(e+f+b-\sqrt{(e+f)^2+b^2+2fb-2eb}\right)/2} \\ B=\sqrt{\left(e+f+b+\sqrt{(e+f)^2+b^2+2fb-2eb}\right)/2} \\ C=e+f-b+\sqrt{(e+f)^2+b^2+2fb-2eb} \\ D=e+f-b-\sqrt{(e+f)^2+b^2+2fb-2eb} \end{cases} \tag{37}$$

According to the first, the third and the last conditions in (35), the coefficients C_3, C_4 and C_5 in (36) are all zero. The coefficients C_1,C_2 and C_6 can be determined by the other conditions in (35). Thus we determine the coefficients in Eq. (36) as

$$\begin{cases} C_1=-2\varepsilon_0(1+\nu_c)[\sqrt{e}\ I_1(B)K_0(\sqrt{e})+B\ I_0(B)K_1(\sqrt{e})]/G \\ C_2=4\varepsilon_0(1+\nu_c)[\sqrt{e}\ I_1(A)K_0(\sqrt{e})+A\ I_0(A)K_1(\sqrt{e})]/G \\ C_3=0 \\ C_4=0 \\ C_5=0 \\ C_6=8f\varepsilon_0(1+\nu_c)[A\ I_1(B)\ I_0(A)-B\ I_1(A)\ I_0(B)]/G \end{cases} \tag{38}$$

where for simplicity, we use the notation $I_\alpha(x)=\mathrm{Bessell}(\alpha,\ x)$ and $K_\alpha(x)=\mathrm{BesselK}(\alpha,\ x)$, where α and x are parameters in Bessel functions; and

$$\begin{aligned} G=&2[2ABC\ I_0(B)\ I_0(A)+(1-\nu_c)AD\ I_1(B)\ I_0(A)+B(\nu_c-1)C\ I_1(A)\ I_0(B)]K_1(\sqrt{e}) \\ &+[D+4C(\nu_c-1)I_1(A)\ I_1(B)+2AC]\sqrt{e}\ K_0(\sqrt{e}) \end{aligned} \tag{39}$$

Substituting (36) into (29) gives the cell traction as

$$\overline{\tau}_c = -\frac{h_c}{R}\left[C_1 A^2 C\text{BesselI}(1, A\overline{r}) + C_2 B^2 D\text{BesselI}(1, B\overline{r})\right] \tag{40}$$

3. Results

3.1. Cell displacement and traction on semi-infinite substrate

3.1.1. Effect of substrate stiffness on cell displacement and traction under constant integrin-ligand bond density

Fig. 4 plots the calculated cell displacement and traction distributions for various stiffness ratios between substrate and cell (the parameters used in the calculations are listed in Table 1). Both cell displacement (Fig. 4a) and traction (Fig. 4b) increase with distance away from the cell center, which is consistent with the relevant experimental observations on the distribution of cell traction on substrate (Gardel et al., 2008; Rape et al., 2011). The distribution of cell traction is also consistent with that of FACs, suggesting that the formation of FACs is regulated by the magnitude of cell traction (Kong et al., 2010). The substrate stiffness is seen to have significant effect on cell displacement and traction. For example, the cell displacement varies with distance linearly on a soft substrate but exponentially on a stiff substrate. The cell traction also varies linearly with distance near the center on a soft substrate, but it rises up dramatically at the cell periphery. It can be seen that our analytical solution is consistent with numerical results when $E_s/E_c > 0.5$. For $E_s/E_c < 0.5$ (substrate substantially softer than the cell itself), the analytical solution becomes inaccurate because the assumption of a small parameter $a < 1$ is no longer valid. The numerical method used is described in Supporting information S3.

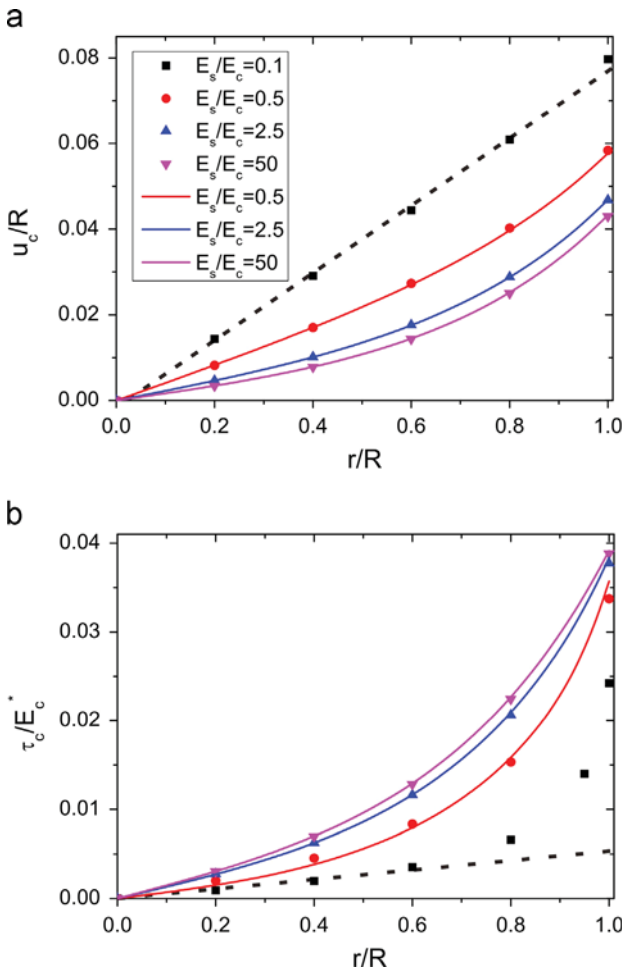

Fig. 4. Radial distributions of cell displacement and traction for various values of substrate stiffness. (a) The cell displacement increases with distance from the cell center, exhibiting a transition from linear to exponential variations at increasing substrate stiffness. (b) The cell traction increases with distance from the cell center. The solid lines stand for analytical solutions and discrete dots are numerical results. Note that no analytical solution is available for the case $E_s/E_c = 0.1$.

Table 1
Main parameters used in the present study.

Parameter	Definition	Value	Source
E_c	Young's modulus of cell	*20 kPa*	Kuznetsova et al. (2007) and Gavara and Chadwick (2012)
ν_c	Poisson's ratio of cell	*0.3*	Trickey et al. (2006)
h_c	Cell height	*2 μm*	Jeanes et al. (2009) and Bottier et al. (2011)
ε_0	Cell pre-strain	*0.1*	(Lu et al., 2008)
R	Cell radius	*20 μm*	Reinhart-King et al. (2005) and Tee et al. (2011)
k_b	Stiffness of integrin-ligand bond	*0.025 nN/μm*	Bell et al. (1984)
ρ	Average density of integrin-ligand bonds on continuum substrate	*40 μm^{-2}*	Arnold et al. (2004)
ρ_p	Bond density of FACs on posts	*400 μm^{-2}*	Chen et al. (2003) and Arnold et al. (2004)
ν_s	Poisson's ratio of substrate	*0.3*	
r_p	Radius of micro-post	*1 μm*	Ghibaudo et al. (2008)
d	Distance micro-post	*4 μm*	Ghibaudo et al. (2008)
h_p	Height of micro-post	*1–12 μm*	Ghibaudo et al. (2008)

To further understand the effect of substrate stiffness, we calculate the cell displacement and traction at the cell periphery as a function of substrate stiffness (Fig. 5). The results show that the peripheral cell displacement is inversely proportional to substrate stiffness for $E_s/E_c < 5$ and asymptotically settles down to a plateau for $E_s/E_c > 5$. In comparison, the cell traction first increases and then levels off to a constant value with increasing substrate stiffness. These results suggest that increase of substrate stiffness can enhance the cell adhesion, but cells will not sense any changes in substrate stiffness once the latter rises above a critical value. Similar conclusions have been reached previously from a simple two-spring model (Schwarz et al., 2006). In this model, the interfacial bonds and substrate are modeled as two elastic springs connected in series, with overall effective stiffness$k_{eff} = k_b k_s/(k_b + k_s)$, k_s being the effective spring constant of the substrate and k_b the effective spring constant of the interfacial bonds. If $k_s \gg k_b$, then $k_{eff} \to k_b$, i.e., the stiffness of the interfacial bond dominates the overall stiffness of the system. In this situation, the cell can hardly sense any changes in substrate stiffness. Recent study demonstrates that the receptors and ligands would form stronger bonds at a stiffer substrate for a more stable cell adhesion compared with the softer one, which provides further evidence for cell's mechanosensing of the substrate elasticity from the molecular level (Li and Ji, 2014).

In addition, our results show that the cell radius R can affect cell traction. For example, the traction at the cell periphery increases linearly with R when $R < 20$ μm and levels off to a plateau when $R > 20$ μm (Fig. 6). This result suggests that cell spreading can promote the growth of FACs through traction enhancement. However, such effect becomes saturated when the cell radius is too large.

3.1.2. *Effect of non-uniform distribution of integrin-ligand bonds on cell displacement and traction*

To consider possible non-uniform distributions of integrin-ligand bonds at the cell–substrate interface, we assume that the bond density ρ is a power function of r as $\rho = (\rho_0(N+2)/2R^N)r^N$ $(N = 0, 1, 2, ..)$. The case $N = 0$ corresponds to a uniform distribution of interfacial bonds with density $\rho = \rho_0$. The total number of bonds is kept constant for different values of N. If we substitute the non-uniform bond distribution into Eq. (16), we obtain the governing equation as

$$\frac{d^2\bar{u}_c(\bar{r})}{d\bar{r}^2} + \frac{1}{\bar{r}}\frac{d\bar{u}_c(\bar{r})}{d\bar{r}} - \left(\frac{1}{\bar{r}^2} + b'\bar{r}^N\right)\bar{u}_c(\bar{r}) - a'\bar{r}^N \int_0^1 f\left(\frac{\bar{r}'}{\bar{r}}\right)\left[\frac{d^2\bar{u}_c(\bar{r}')}{d\bar{r}'^2} + \frac{1}{\bar{r}'}\frac{d\bar{u}_c(\bar{r}')}{d\bar{r}'} - \frac{1}{\bar{r}'^2}\bar{u}_c(\bar{r}')\right] d\bar{r}' = 0 \tag{41}$$

where $a' = \frac{(N+2)\rho_0 k_b R}{\pi E_s^*}$ and $b' = \frac{(N+2)\rho_0 k_b R^2}{2E_c^* h_c}$.

The zeroth-order perturbation solution is

$$\bar{u}_{c(0)}(\bar{r}) = C'_{1(0)}\text{Bessell}\left(\frac{1}{\lambda}, \frac{\sqrt{b'}}{\lambda}\bar{r}^\lambda\right) + C'_{2(0)}\text{BesselK}\left(\frac{1}{\lambda}, \frac{\sqrt{b'}}{\lambda}\bar{r}^\lambda\right) \tag{42}$$

where $\lambda = (N+2)/2$. Substituting (42) into (20), the coefficients $C'_{1(0)}$ and $C'_{2(0)}$ can be determined as

$$\begin{cases} C'_{1(0)} = \dfrac{\varepsilon_0(1+\nu_c)}{(1-\nu_c)\text{Bessell}\left(\frac{1}{\lambda}, \frac{\sqrt{b'}}{\lambda}\right) - \sqrt{b'}\text{Bessell}\left(\frac{1}{\lambda}-1, \frac{\sqrt{b'}}{\lambda}\right)} \\ C'_{2(0)} = 0 \end{cases} \tag{43}$$

Higher-orders perturbation solutions can be obtained using numerical methods. Fig. 7 shows the effect of power exponent N on the distributions of cell displacement and traction. At increasing N, more interfacial bonds become concentrated at the cell periphery, cell displacement is reduced near the edge (Fig. 7a) and cell traction is decreased in the

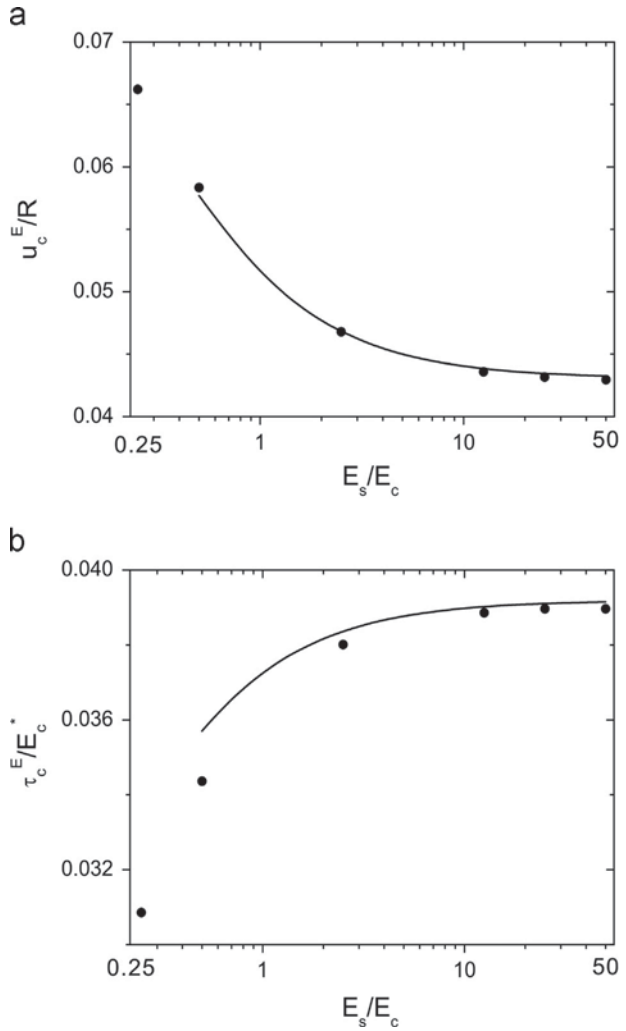

Fig. 5. Effect of substrate stiffness on the cell displacement and traction at cell periphery. (a) The cell displacement is inversely proportional to substrate stiffness when $E_s/E_c < 5$, but it decreases to a plateau value when $E_s/E_c > 5$. (b) The cell traction is seen to be proportional to substrate stiffness on soft substrates, but levels off to a constant value on stiff substrates. The solid lines stand for analytical solutions and discrete dots are numerical results.

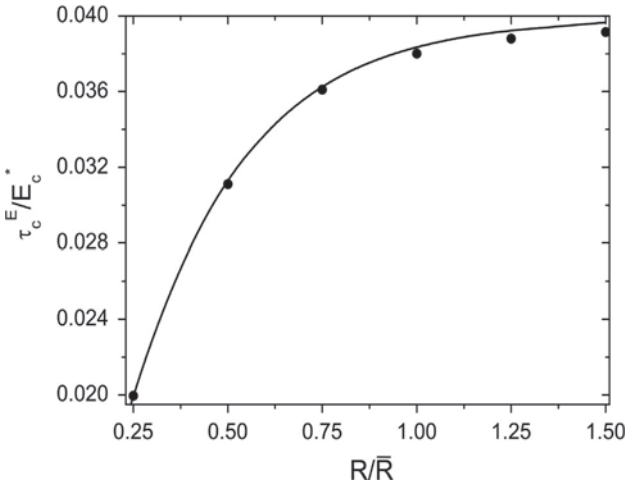

Fig. 6. Effect of cell size on cell traction. The traction at the cell periphery increases linearly with cell size R when $R < 20$ μm, but it reaches a plateau value when $R > 20$ μm. Here $E_s/E_c = 2.5$ and $\bar{R} = 20$ μm. The solid lines stand for analytical solutions and discrete dots are numerical results.

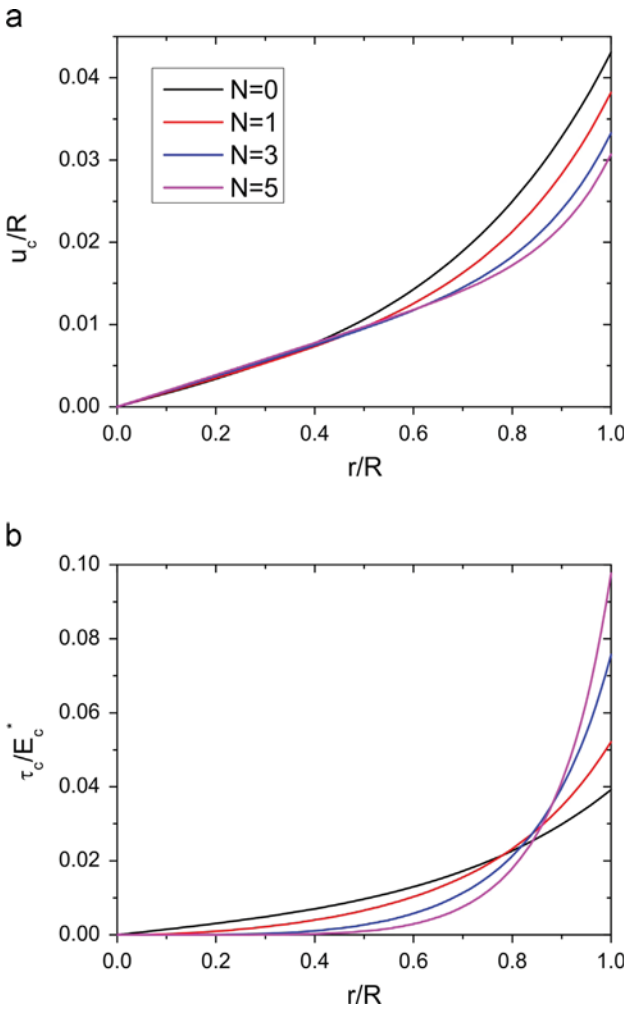

Fig. 7. Effect of a power-law distribution of bond density on the cell displacement and traction. Increasing power exponent N reduces (a) the cell displacement and (b) cell traction in the interior region, while it significantly increases the traction at cell periphery.

cell interior but increased at the cell periphery (Fig. 7b). This suggests that localization of FACs at cell periphery tends to promote cell spreading.

3.1.3. *Substrate with microposts*

Micropost-patterned substrates have been widely used in the measurements of cell traction forces. The magnitude of cell traction can be estimated by measuring the deflection of the micro-posts. For small deformation, the cell traction force on a post is proportional to its deflection δ, i.e., $f=(3E_sI_p/{h_p}^3)\delta$. Therefore, the micro-posts can be thought of as a system of distributed elastic springs with spring constant $k_p=(3E_sI_p/{h_p}^3)$, where h_p is the height and I_p is the cross-section moment of inertia of the posts. For short posts, the spring constant is modified as $\frac{1}{k_p}=\frac{h_p}{3E_s}\left(\frac{{h_p}^2}{I_p}+\frac{7+6\nu_s}{A_p}\right)$ (Schoen et al., 2010). The combined spring constant of a post and the attached molecular bonds is $k_{p+b}=k'_bk_p/(k'_b+k_p)$, where $k'_b=\rho_pk_bA_p$, ρ_p being the bond density and A_p the cross-section area of the post. For a square array of micro-posts, the post density is $\rho_{p+b}=(1/d^2)$.

Replacing ρk_b with $\rho_{p+b}k_{p+b}$ in Eq. (16), the cell displacement and traction on a micropost patterned substrate is calculated and shown in Fig. 8a and b, respectively. Clearly, the height of the posts strongly affects the cell displacement and traction. The cell traction varies with distance from the cell center linearly at large post height h_p and exponentially at small h_p. Compared to the case of a continuous substrate, the traction on high posts is proportional to distance from the cell center over the whole cell domain, with no concentration at the cell periphery. This suggests that a continuous substrate is better for promoting the formation of FACs at cell periphery.

In addition, the above traction–distance law, which is found for micro-posted as well as continuous substrates, is consistent with experimental observations of cells on micro-posted substrates by Ladoux et al. (Saez et al., 2005; Ghibaudo et al., 2008; Ladoux et al., 2010). Our results also indicate that the assumption of cell traction being linearly proportional to

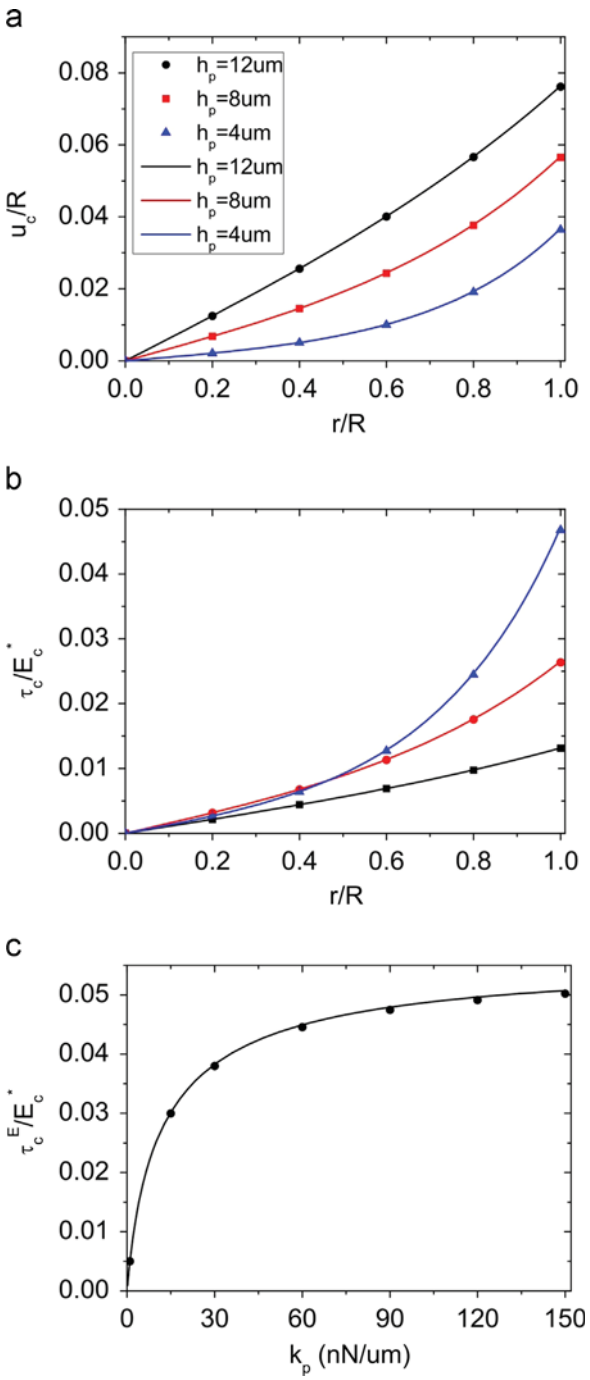

Fig. 8. Radial distributions of cell displacement and traction at various values of the micro-post height h_p on a micro-post patterned substrate. (a) The cell displacement increases with distance from the cell center. (b) The cell traction increases with distance from the cell center. The traction–distance relationship changes from linear to exponential as h_p is reduced. (c) The cell traction at cell periphery exhibits a biphasic dependence on substrate stiffness, i.e., it increases linearly with the stiffness of the micro-posts when the latter is low and levels off to a constant value when it is high.

distance from the cell center (Lemmon and Romer, 2010) is applicable only for cells on a soft matrix. The saturation of cell traction force (Fig. 8c) on sufficiently stiff pillars is also consistent with the experimental measurements by Ladoux and co-workers (Saez et al., 2005; Ghibaudo et al., 2008; Ladoux et al., 2010).

3.1.4. *Characteristic decay distance of cell induced deformation*

Next we calculate the radial displacement $u'_s(r,z)$ and shear stress $\tau_{zr}(r,z)$ in the substrate as functions of depth z by using the Boussinesq–Cerruti solution (see Supporting information S1). Fig. 9a and b show the variations of $u'_s(r,z)$ and

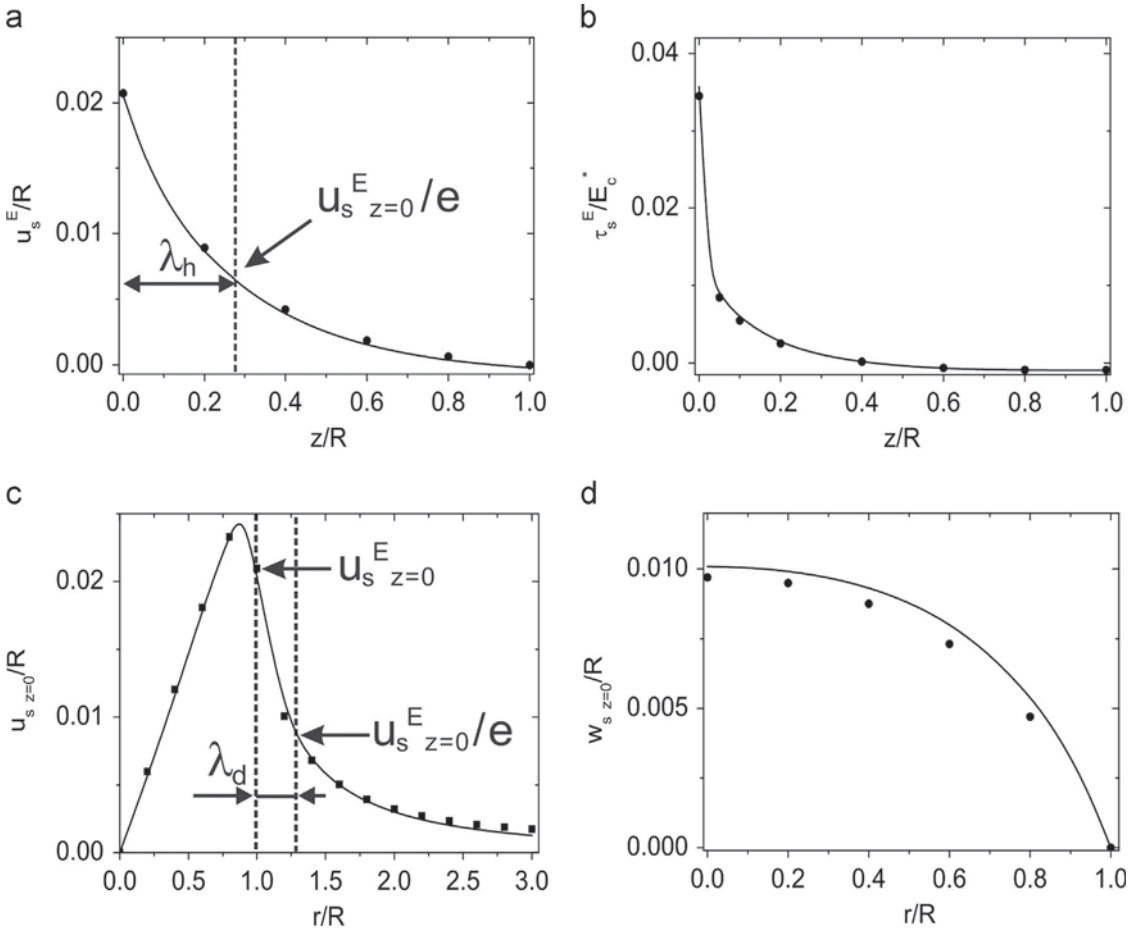

Fig. 9. Cell-induced radial displacement and shear stress in the substrate. The variations of (a) radial displacement and (b) shear stress at the cell edge with depth z into the substrate, λ_h being the characteristic depth of decay. (c) The variation of radial displacement on the substrate surface with distance from the cell center, λ_d being the characteristic distance of decay from the cell edge. (d) The out-of-plane displacement w_s in the cell domain. Here $E_s/E_c = 0.5$.

$\tau_{zr}(r,z)$ with depth z at cell periphery. It can be seen that both $u'_s(r,z)$ and $\tau_{zr}(r,z)$ decay with depth and approach zero when $z > R$, indicating that the substrate can be treated as a half-space once its height is larger than the cell radius. Furthermore, the radial displacement at the substrate surface, $u'_s(r,0)$, exhibits similar exponential decay with distance away from the cell edge for $r > R$ (see Fig. 9c). Fig. 9d plots the vertical displacement $w'_s(r,0)$ of the substrate surface as a function of the radial distance from the cell center, showing a concave substrate surface profile in the presence of a cell, which is again consistent with experimental observations (Delanoe-Ayari et al., 2010).

Fig 9a and c suggests that we can estimate the depth and distance of cell sensing from the characteristic decay length of cell-induced substrate deformation. The characteristic length associated with depth decay, λ_h, is defined as the depth at which the substrate displacement decays to $1/e$ times that at the cell edge, while the characteristic length associated with lateral decay, λ_d, is defined as the lateral distance away from the cell edge (see also Fig. 1c) at which the surface displacement decays to $1/e$ times that at the cell edge. The decay depth and distance remain almost constant with respect to the substrate stiffness (Fig. 10a), and vary almost linearly with the cell size (Fig. 10b). If we define the cell sensing depth L_h as the depth at which the cell-induced substrate displacement decays to 0.01 times that at the surface, and cell sensing distance L_d as the distance from the cell edge at which the surface displacement decays to 0.01 times that at the cell edge, it can be shown that $L_h = \beta\lambda_h$ and $L_d = \beta\lambda_d$, where $\beta = 2\ln 10$. It follows from these definitions that the characteristic length for mechanosensing of cells on substrates is roughly equal to the cell radius, with $L_h = 1.15R$ and $L_d = 1.38R$.

3.2. *Effect of substrate thickness*

The cell displacement and traction on a substrate of finite thickness can be calculated from Eqs. (36, 40). Fig. 11 shows that the thickness of the substrate strongly affects the deformation and traction fields in both cell and substrate when the former is less than a critical length, and there is a good consistency between the analytical solutions and FEM results. The cell traction varies approximately linearly with distance from the cell center within the inner cell region, while

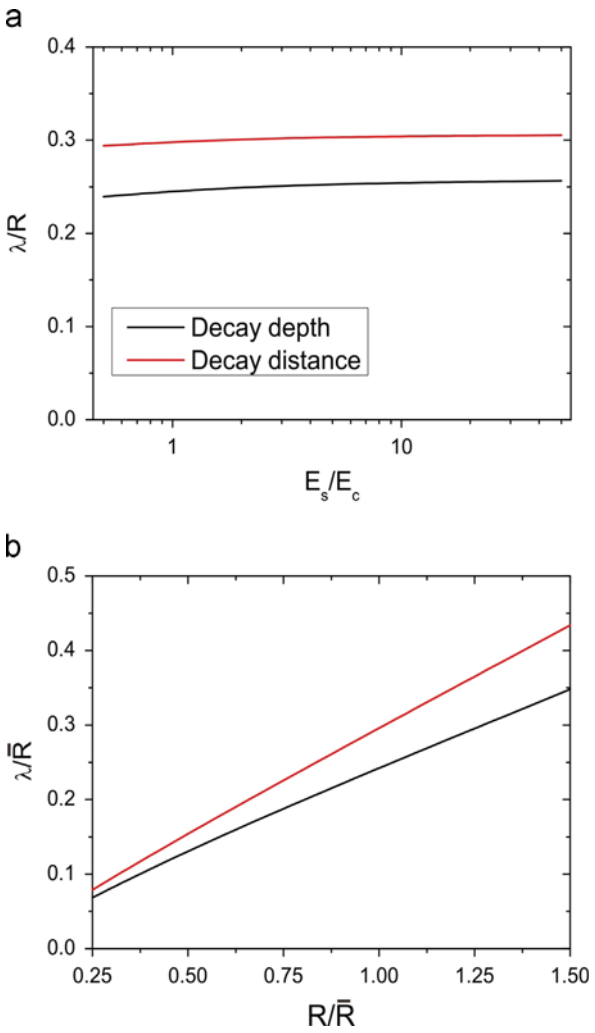

Fig. 10. Mechanosensing distance of cells measured from the characteristic length of decay in cell induced deformation in an elastic substrate. The characteristic decay depth and distance versus (a) substrate stiffness and (b) cell size. Here $\bar{R}=20$ um.

concentrating at the cell edge (Fig. 11a). In addition, with increasing substrate thickness, the traction at the cell periphery decreases but the displacement increases, and both level off to their half-space values when $H/R>1$; see Fig. 11(b and c). These results are consistent with the experiments of Sen et al. (2009) that showed enhanced cell spreading and less contraction of mesenchymal stem cells on thin gels compared to those on thick ones.

4. Discussion

4.1. Cell traction distribution versus driving force for cell migration

Our analysis shows that the cell traction increases either linearly or exponentially with distance from the cell center, depending on the stiffness of the substrate (Fig. 4b and Fig. 8b). This result, which is consistent with experimental measurements, has important implications on the production and regulation of the driving force for cell migration.

The shape of a migrating cell is usually polarized (Zhong et al., 2014). For example, migrating fibroblasts exhibit a large front (lamellipodia) and a long tail. In this configuration, the area of cell front is much larger than the tail, and the cell center is located closer to the front (Dembo and Wang, 1999). According to the traction–distance law, the larger the distance from the cell center, the higher the cell traction. Therefore, the traction should be larger at the cell tail than at the front. Polarized keratocytes have a crescent-like shape consisting of a large front and two flank-like rears at cell sides (Burton et al., 1999), and the cell center is also closer to the front. This profile again induces larger traction forces at the cell rear than at the front.

The above predictions are consistent with experimentally measured traction distributions in fibroblasts and keratocytes (Burton et al., 1999; Dembo and Wang, 1999; Wang et al., 2001; Fournier et al., 2010). The experiments showed that cell traction is smaller at the cell front than at the rear. This traction distribution profile is critical for cell migration. At the cell

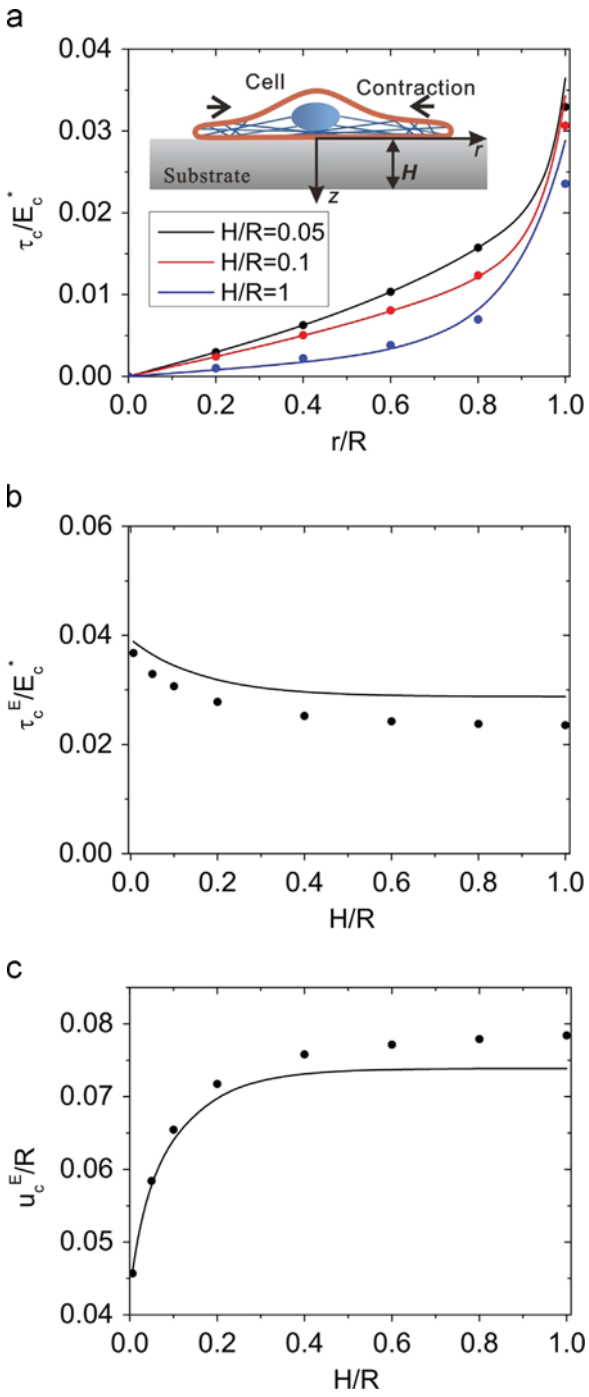

Fig. 11. Effect of substrate thickness on cell displacement and traction. (a) The cell traction increases with distance from the cell center at different values of the substrate thickness. The biphasic dependence of (b) cell traction and (c) displacement at the cell edge on the substrate thickness. The solid lines stand for analytical solutions and discrete dots are FEM results. Here $E_s/E_c = 0.1$.

front, the relatively small traction is expected to promote the formation of FACs (Kong et al., 2010), while the large traction at the cell rear induces disassembly of FACs (Kong et al., 2008b), causing detachment of the cell rear so as to provide a driving force for cell migration (Zhong and Ji, 2013).

These results also suggest that cell shape could be used to control cell motility, as different cell shapes induce different distributions of cell traction. It has been recently shown that cell shape plays a pivotal role in cell migration by regulating cell traction at cell front and rear: the higher the cell polarity, the higher the driving force for cell migration (Zhong and Ji, 2013, 2014).

4.2. Do cells sense force or deformation of their substrates?

A long pursued, debated and frequently asked question is whether cells sense force or deformation in their microenvironment. Saez et al. (2005) showed that the traction forces of epithelial cell are linearly proportional to substrate rigidity, suggesting that the cellular forces are regulated by the deformation of the matrix in trying to maintain a homeostatic strain. However, the measurements by Freyman et al. (2002) showed that the cell traction is limited by the force rather than the displacement of the medium. These seemingly conflicting experimental results give rise to a puzzle on whether cellular activity is controlled by force/stress or deformation/strain in the medium.

This puzzle suggests that there is no simple monotonic relationship between cell traction and substrate stiffness. We note that the substrate stiffness used in Freyman et al. (2002) is much higher than that in Saez et al. (2005). According to our analysis, the cell traction increases linearly with substrate stiffness on a soft substrate, but it levels off to a constant value on a stiff substrate (Figs. 5b and 8c). This suggests that cell would appear to maintain constant strain on soft substrates and constant traction on stiff substrates.

This finding can be extended to different cell types. Ghibaudo et al. (2008) showed that cell traction exhibits a biphasic dependence on the stiffness of micro-posts for fibroblasts and epithelial cells. They found a linear regime in the traction-stiffness relation when the stiffness of the micro-posts is below a critical value, suggesting a constant value of post deflection of around 100 nm for fibroblasts and 160 nm for epithelial cells. Above a critical value of micro-post stiffness, they observed a second regime with a constant traction of 11 nN for fibroblasts and 18 nN for epithelial cells.

The biphasic dependence of cell traction on substrate stiffness observed by Ghibaudo et al. (2008) is consistent with our predictions for cells on both continuous and micro-post patterned substrates. We have seen that the cell traction on both continuous and micro-post patterned substrates levels off to a plateau value when the substrate stiffness rises above a critical value (Figs. 5b and 8c). This result can also be reached from the two-spring model of Schwarz et al. (2006). According to the model, the effective stiffness of the system is dominated by the substrate stiffness $k_{eff} \approx k_s$ when $k_s \ll k_b$, in which case the cell traction will be sensitive to the substrate stiffness, but when $k_s \gg k_b$, we have $k_{eff} \approx k_b$, in which case the stiffness of substrate has little effect on the flexibility of the system. Therefore, there is no unique answer to the question of whether cells feel the deformation or force because of the biphasic dependence of cell traction on substrate stiffness.

4.3. How far can cells sense into their substrates?

Our results show that the displacement and stress of substrate decay exponentially with depth and distance from the cell. They both approach zero when the depth is around the cell radius (Fig. 9a and b). This behavior is related to the question how far do cells feel into their microenvironment (Sen et al., 2009). According to our analysis, the cell induced displacement and stress field in the substrate essentially vanish beyond a critical depth and distance comparable to the cell size, which provides a clear definition on how far cells can feel into their substrates. This mechanosensing length is not sensitive to the substrate stiffness in the range of $0.5 < E_s/E_c < 50$, in consistency with experimental observations (Merkel et al., 2007).

An interesting observation about cellular mechanosensing is that bone cells (osteocyte, osteoblast and osteoclast) sense mechanical signals associated with bone remodeling: osteoblasts and osteoclasts are normally at the bone surface while osteocytes are embedded in the bone matrix. In this problem, it is important to know how far the cells can sense mechanical stimuli (Wang et al., 2012, 2014). In the literature on bone modeling simulation (Ruimerman et al., 2005), the mechanosensing length is often taken to be 100 μm, which is on the same order of magnitude as the value predicted by our model.

This result also suggests that a substrate thicker than the cell radius can be approximately treated as a semi-infinite substrate (Maloney et al., 2008), which is crucial to the experimental measurement of cell traction forces from the associated surface deformation of a substrate of finite thickness. Our analysis indicates that the thickness of the substrate should be chosen larger than the mechanosensing length if the traction force is to be determined from an inverse method based on the Boussinesq–Cerruti solution of a semi-infinite substrate.

5. Conclusions

A simple mechanics model of mechnosensing of cells on elastic substrates has been developed. In this model, the cell is modeled as a pre-strained circular disk on an elastic substrate. Analytical and numerical solutions have been obtained for the cell traction and induced displacements in cell and substrate. We showed that the magnitude and distribution of cell traction depend on substrate stiffness, substrate thickness, interfacial bond density and cell size. The main results are summarized as follows:

- It is shown that the cell traction generally increases with distance from the cell center. This traction distribution law suggests important roles of cell shape (polarization) in regulating the speed and direction of cell migration.
- Substrate stiffness has significant influence on the distribution and magnitude of cell traction, which changes from a linear distribution with distance from the cell center on a soft substrate to an exponential distribution on a stiff substrate.

It is found that the maximum cell traction exhibits a biphasic dependence on substrate stiffness: it increases linearly with the stiffness of a soft substrate (corresponding to a constant deformation/strain), and then levels off to a constant value on a stiff substrate. These results suggest that cells mainly sense deformation on a soft substrate but force on a stiff substrate.

- It is found that the elastic displacement in the substrate decays with distance away from the cell edge, as well as with depth from the surface. The characteristic decay length for the elastic field has been related to the mechanosensing length of cells, which is shown to be comparable to the cell size. Our results show that the mechanosensing length of cells is insensitive to substrate stiffness.

While the present study has provided some insights into mechanosensing of cells on elastic substrates, a number of open questions can be further explored in the future work:

- It will be interesting to study the underlying mechanisms that control the magnitude of cell's eigenstrain which is around 0.1 according to existing experiments (Deguchi et al., 2006; Lu et al., 2008). Many studies in the literature (Bayraktar and Keaveny, 2004; Guo et al., 2005; Arampatzis et al., 2007) suggest that there exist homeostatic eigenstrains even at the level of macroscale tissues such as bone, tendon or blood vessel. However, the underlying mechanisms, which seem to involve many length scales from molecular, subcellular to cellular scales, that determine the value of the eigenstrains in cells and tissues remain to be fully clarified.
- It will be interesting to study the effect of cell–cell interactions on mechanosensing. In the present study, we only considered single cell behaviors. The cell–cell interaction is expected to influence cell–substrate interaction. Experiments showed that for the metastasis of tumor cells, the cell–cell adhesion is dramatically reduced to allow for invasive migration of tumor cells.
- It will also be interesting to study the distribution of cell traction and associated deformation on anisotropic and spatially constrained substrate, as well as their effect on the driving force of cell migration.

Acknowledgment

This research was supported by the National Natural Science Foundation of China through Grant nos. 11025208, 11372042 and 11221202. The work of HG has been supported by NSF through grant CMMI-1028530 and the Center for Mechanics and Materials at Tsinghua University.

Appendix A. Supporting information

Supplementary data associated with this article can be found in the online version at http://dx.doi.org/10.1016/j.jmps.2014.05.016.

References

Arampatzis, A., Karamanidis, K., Albracht, K., 2007. Adaptational responses of the human Achilles tendon by modulation of the applied cyclic strain magnitude. J. Exp. Biol. 210 (15), 2743–2753.
Arnold, M., Cavalcanti-Adam, E.A., Glass, R., Blummel, J., Eck, W., Kantlehner, M., Kessler, H., Spatz, J.P., 2004. Activation of integrin function by nanopatterned adhesive interfaces. ChemPhysChem 5 (3), 383–388.
Balaban, N.Q., Schwarz, U.S., Riveline, D., Goichberg, P., Tzur, G., Sabanay, I., Mahalu, D., Safran, S.A., Bershadsky, A., Addadi, L., Geiger, B., 2001. Force and focal adhesion assembly: a close relationship studied using elastic micropatterned substrates. Nat. Cell Biol. 3 (5), 466–472.
Bayraktar, H.H., Keaveny, T.M., 2004. Mechanisms of uniformity of yield strains for trabecular bone. J. Biomech. 37 (11), 1671–1678.
Bell, G.I., Dembo, M., Bongrand, P., 1984. Cell adhesion. Competition between nonspecific repulsion and specific bonding. Biophys. J. 45 (6), 1051–1064.
Bershadsky, A.D., Balaban, N.Q., Geiger, B., 2003. Adhesion-dependent cell mechanosensitivity. Annu. Rev. Cell Dev. Biol. 19, 677–695.
Bischofs, I.B., Safran, S.A., Schwarz, U.S., 2004. Elastic interactions of active cells with soft materials. Phys. Rev. E 69, 021911.
Bottier, C., Gabella, C., Vianay, B., Buscemi, L., Sbalzarini, I.F., Meister, J.-J., Verkhovsky, A.B., 2011. Dynamic measurement of the height and volume of migrating cells by a novel fluorescence microscopy technique. Lab Chip 11 (22), 3855–3863.
Burton, K., Park, J.H., Taylor, D.L., 1999. Keratocytes generate traction forces in two phases. Mol. Biol. Cell 10 (11), 3745–3769.
Butler, J.P., Tolic-Norrelykke, I.M., Fabry, B., Fredberg, J.J., 2002. Traction fields, moments, and strain energy that cells exert on their surroundings. AJP: Cell Physiol. 282 (3), C595–C605.
Chen, B., Gao, H., 2010. Mechanical principle of enhancing cell-substrate adhesion via pre-tension in the cytoskeleton. Biophys. J. 98 (10), 2154–2162.
Chen, B., Kemkemer, R., Deibler, M., Spatz, J., Gao, H., 2012. Cyclic stretch induces cell reorientation on substrates by destabilizing catch bonds in focal adhesions. Plos One 7 (11), e48346.
Chen, C.S., Alonso, J.L., Ostuni, E., Whitesides, G.M., Ingber, D.E., 2003. Cell shape provides global control of focal adhesion assembly. Biochem. Biophys. Res. Commun. 307 (2), 355–361.
Chen, S., Gao, H., 2006. Non-slipping adhesive contact between mismatched elastic spheres: a model of adhesion mediated deformation sensor. J. Mech. Phys. Solids 54 (8), 1548–1567.
De, R., Safran, S.A., 2008. Dynamical theory of active cellular response to external stress. Phys. Rev. E 78 (3), 031923.
De, R., Zemel, A., Safran, S.A., 2007. Dynamics of cell orientation. Nat. Phys. 3 (9), 655–659.
De, R., Zemel, A., Safran, S.A., 2008. Do cells sense stress or strain? Measurement of cellular orientation can provide a clue. Biophys. J. 94 (5), L29–L31.

Deguchi, S., Ohashi, T., Sato, M., 2006. Tensile properties of single stress fibers isolated from cultured vascular smooth muscle cells. J. Biomech. 39 (14), 2603–2610.
Delanoe-Ayari, H., Rieu, J.P., Sano, M., 2010. 4D traction force microscopy reveals asymmetric cortical forces in migrating dictyostelium cells. Phys. Rev. Lett. 105 (24), 248103.
Dembo, M., Wang, Y.L., 1999. Stresses at the cell-to-substrate interface during locomotion of fibroblasts. Biophys. J. 76 (4), 2307–2316.
Deshpande, V.S., Mrksich, M., McMeeking, R.M., Evans, A.G., 2008. A bio-mechanical model for coupling cell contractility with focal adhesion formation. J. Mech. Phys. Solids 56 (4), 1484–1510.
Discher, D.E., Janmey, P., Wang, Y.-l., 2005. Tissue cells feel and respond to the stiffness of their substrate. Science 310, 1139–1144.
Edwards, C.M., Schwarz, U.S., 2011. Force localization in contracting cell layers. Phys. Rev. Lett. 107 (12), 128101.
Engler, A.J., Richert, L., Wong, J.Y., Picart, C., Discher, D.E., 2004. Surface probe measurements of the elasticity of sectioned tissue, thin gels and polyelectrolyte multilayer films: correlations between substrate stiffness and cell adhesion. Surf. Sci. 570 (1–2), 142–154.
Engler, A.J., Sen, S., Sweeney, H.L., Discher, D.E., 2006. Matrix elasticity directs stem cell lineage specification. Cell 126 (4), 677–689.
Fournier, M.F., Sauser, R., Ambrosi, D., Meister, J.-J., Verkhovsky, A.B., 2010. Force transmission in migrating cells. J. Cell Biol. 188 (2), 287–297.
Freyman, T.M., Yannas, I.V., Yokoo, R., Gibson, L.J., 2002. Fibroblast contractile force is independent of the stiffness which resists the contraction. Exp. Cell Res. 272 (2), 153–162.
Friedrich, B.M., Safran, S.A., 2012. How cells feel their substrate: spontaneous symmetry breaking of active surface stresses. Soft Matter 8 (11), 3223–3230.
Fu, J., Wang, Y.-K., Yang, M.T., Desai, R.A., Yu, X., Liu, Z., Chen, C.S., 2010. Mechanical regulation of cell function with geometrically modulated elastomeric substrates. Nat. Methods 7 (9), 733–736.
Gardel, M.L., Sabass, B., Ji, L., Danuser, G., Schwarz, U.S., Waterman, C.M., 2008. Traction stress in focal adhesions correlates biphasically with actin retrograde flow speed. J. Cell Biol. 183 (6), 999–1005.
Gavara, N., Chadwick, R.S., 2012. Determination of the elastic moduli of thin samples and adherent cells using conical atomic force microscope tips. Nat. Nanotechnol. 7 (11), 733–736.
Ghassemi, S., Meacci, G., Liu, S., Gondarenko, A.A., Mathur, A., Roca-Cusachs, P., Sheetz, M.P., Hone, J., 2012. Cells test substrate rigidity by local contractions on submicrometer pillars. Proc. Natl. Acad. Sci. USA 109 (14), 5328–5333.
Ghibaudo, M., Saez, A., Trichet, L., Xayaphoummine, A., Browaeys, J., Silberzan, P., Buguin, A., Ladoux, B., 2008. Traction forces and rigidity sensing regulate cell functions. Soft Matter 4 (9), 1836–1843.
Guo, X., Lu, X., Kassab, G.S., 2005. Transmural strain distribution in the blood vessel wall. Am. J. Physiol. Heart Circ. Physiol. 288 (2), H881–H886.
Harris, A.K., Wild, P., Stopak, D., 1980. Silicone rubber substrata: a new wrinkle in the study of cell locomotion. Science 208 (4440), 177–179.
Jeanes, A., Smutny, M., Leerberg, J.M., Yap, A.S., 2009. Phosphatidylinositol 3′-kinase signalling supports cell height in established epithelial monolayers. J. Mol. Histol. 40 (5–6), 395–405.
Johnson, K.L., 1987. Contact Mechanics. Cambridge University Press, Cambridge.
Jungbauer, S., Gao, H., Spatz, J.P., Kemkemer, R., 2008. Two characteristic regimes in frequency-dependent dynamic reorientation of fibroblasts on cyclically stretched substrates. Biophys. J. 95 (7), 3470–3478.
Kaunas, R., Nguyen, P., Usami, S., Chien, S., 2005. From the cover: cooperative effects of Rho and mechanical stretch on stress fiber organization. Proc. Natl. Acad. Sci. USA 102, 15895–15900.
Kong, D., Ji, B., Dai, L., 2008a. Nonlinear mechanical modeling of cell adhesion. J. Theor. Biol. 250 (1), 75–84.
Kong, D., Ji, B., Dai, L., 2008b. Stability of adhesion clusters and cell reorientation under lateral cyclic tension. Biophys. J. 95 (8), 4034–4044.
Kong, D., Ji, B.H., Dai, L.H., 2010. Stabilizing to disruptive transition of focal adhesion response to mechanical forces. J. Biomech. 43 (13), 2524–2529.
Kuznetsova, T.G., Starodubtseva, M.N., Yegorenkov, N.I., Chizhik, S.A., Zhdanov, R.I., 2007. Atomic force microscopy probing of cell elasticity. Micron 38 (8), 824–833.
Ladoux, B., Anon, E., Lambert, M., Rabodzey, A., Hersen, P., Buguin, A., Silberzan, P., Mege, R.-M., 2010. Strength dependence of cadherin-mediated adhesions. Biophys. J. 98 (4), 534–542.
Legant, W.R., Miller, J.S., Blakely, B.L., Cohen, D.M., Genin, G.M., Chen, C.S., 2010. Measurement of mechanical tractions exerted by cells in three-dimensional matrices. Nat. Methods 7 (12), 969–971.
Lemmon, C.A., Romer, L.H., 2010. A predictive model of cell traction forces based on cell geometry. Biophys. J. 99 (9), L78–L80.
Li, D., Ji, B., 2014. Predicted rupture force of a single molecular bond becomes rate independent at ultralow loading rates. Phys. Rev. Lett. 112 (7), 078302.
Liu, B., Qu, M.-J., Qin, K.-R., Li, H., Li, Z.-K., Shen, B.-R., Jiang, Z.-L., 2008. Role of cyclic strain frequency in regulating the alignment of vascular smooth muscle cells in vitro. Biophys. J. 94 (4), 1497–1507.
Lo, C.-M., Wang, H.-B., Dembo, M., Wang, Y.-L., 2000. Cell movement is guided by the rigidity of the substrate. Biophys. J. 79 (1), 144–152.
Lu, L., Feng, Y.F., Hucker, W.J., Oswald, S.J., Longmore, G.D., Yin, F.C.P., 2008. Actin stress fiber pre-extension in human aortic endothelial cells. Cell Motil. Cytoskelet. 65 (4), 281–294.
Maloney, J., Walton, E., Bruce, C., Van Vliet, K., 2008. Influence of finite thickness and stiffness on cellular adhesion-induced deformation of compliant substrata. Phys. Rev. E 78 (4), 041923.
Merkel, R., Kirchgessner, N., Cesa, C.M., Hoffmann, B., 2007. Cell force microscopy on elastic layers of finite thickness. Biophys. J. 93 (9), 3314–3323.
Mertz, A.F., Banerjee, S., Che, Y., German, G.K., Xu, Y., Hyland, C., Marchetti, M.C., Horsley, V., Dufresne, E.R., 2012. Scaling of traction forces with the size of cohesive cell colonies. Phys. Rev. Lett. 108 (19), 198101.
Nicolas, A., Safran, S.A., 2006. Limitation of cell adhesion by the elasticity of the extracellular matrix. Biophys. J. 91 (1), 61–73.
Pathak, A., Deshpande, V.S., McMeeking, R.M., Evans, A.G., 2008. The simulation of stress fibre and focal adhesion development in cells on patterned substrates. J. R. Soc. Interface 5 (22), 507–524.
Peyton, S.R., Putnam, A.J., 2005. Extracellular matrix rigidity governs smooth muscle cell motility in a biphasic fashion. J. Cell. Physiol. 204 (1), 198–209.
Polio, S.R., Rothenberg, K.E., Stamenović, D., Smith, M.L., 2012. A micropatterning and image processing approach to simplify measurement of cellular traction forces. Acta Biomater. 8 (1), 82–88.
Qian, J., Liu, H., Lin, Y., Chen, W., Gao, H., 2013. A mechanochemical model of cell reorientation on substrates under cyclic stretch. Plos One 8 (6), e65864.
Rape, A.D., Guo, W.-H., Wang, Y.-L., 2011. The regulation of traction force in relation to cell shape and focal adhesions. Biomaterials 32 (8), 2043–2051.
Reinhart-King, C.A., Dembo, M., Hammer, D.A., 2005. The dynamics and mechanics of endothelial cell spreading. Biophys. J. 89 (1), 676–689.
Riveline, D., Zamir, E., Balaban, N.Q., Schwarz, U.S., Ishizaki, T., Narumiya, S., Kam, Z., Geiger, B., Bershadsky, A.D., 2001. Focal contacts as mechanosensors: externally applied local mechanical force induces growth of focal contacts by an mDia1-dependent and ROCK-independent mechanism. J. Cell Biol. 153 (6), 1175–1186.
Ruimerman, R., Hilbers, P., van Rietbergen, B., Huiskes, R., 2005. A theoretical framework for strain-related trabecular bone maintenance and adaptation. J. Biomech. 38 (4), 931–941.
Saez, A., Buguin, A., Silberzan, P., Ladoux, B., 2005. Is the mechanical activity of epithelial cells controlled by deformations or forces? Biophys. J. 89 (6), L52–L54.
Schoen, I., Hu, W., Klotzsch, E., Vogel, V., 2010. Probing cellular traction forces by micropillar arrays: contribution of substrate warping to pillar deflection. Nano Lett. 10 (5), 1823–1830.
Schwarz, U.S., Erdmann, T., Bischofs, I.B., 2006. Focal adhesions as mechanosensors: the two-spring model. Biosystems 83 (2–3), 225–232.
Schwarz, U.S., Safran, S.A., 2002. Elastic interactions of cells. Phys. Rev. Lett. 88 (4), 048102.
Sen, S., Engler, A.J., Discher, D.E., 2009. Matrix strains induced by cells: computing how far cells can feel. Cell. Mol. Bioeng. 2 (1), 39–48.
Tan, J.L., Tien, J., Pirone, D.M., Gray, D.S., Bhadriraju, K., Chen, C.S., 2003. Cells lying on a bed of microneedles: an approach to isolate mechanical force. Proc. Natl. Acad. Sci. USA 100 (4), 1484–1489.

Tee, S.-Y., Fu, J., Chen, C.S., Janmey, P.A., 2011. Cell shape and substrate rigidity both regulate cell stiffness. Biophys. J. 100 (5), L25–L27.
Trickey, W.R., Baaijens, F.P.T., Laursen, T.A., Alexopoulos, L.G., Guilak, F., 2006. Determination of the Poisson's ratio of the cell: recovery properties of chondrocytes after release from complete micropipette aspiration. J. Biomech. 39 (1), 78–87.
Vlasov, V.Z., Leonten, N.N., 1966. Beams plates and shells on elastic foundations. The Israel Program for Scientific Translations, Tel Aviv.
Wang, H., Ji, B., Liu, X.S., Guo, X.E., Huang, Y., Hwang, K.-C., 2012. Analysis of microstructural and mechanical alterations of trabecular bone in a simulated three-dimensional remodeling process. J. Biomech. 45 (14), 2417–2425.
Wang, H., Ji, B., Liu, X.S., Oers, R.F.M., Guo, X.E., Huang, Y., Hwang, K.-C., 2014. Osteocyte-viability-based simulations of trabecular bone loss and recovery in disuse and reloading. Biomech. Model. Mechanobiol. 13 (1), 153–166.
Wang, H.B., Dembo, M., Hanks, S.K., Wang, Y.L., 2001. Focal adhesion kinase is involved in mechanosensing during fibroblast migration. Proc. Natl. Acad. Sci. USA 98 (20), 11295–11300.
Weng, S., Fu, J., 2011. Synergistic regulation of cell function by matrix rigidity and adhesive pattern. Biomaterials 32 (36), 9584–9593.
Yeung, T., Georges, P.C., Flanagan, L.A., Marg, B., Ortiz, M., Funaki, M., Zahir, N., Ming, W.Y., Weaver, V., Janmey, P.A., 2005. Effects of substrate stiffness on cell morphology, cytoskeletal structure, and adhesion. Cell Motil. Cytoskelet. 60 (1), 24–34.
Zhong, Y., He, S., Dong, C., Ji, B., Hu, G., 2014. Cell polarization energy and its implications for cell migration. Comptes Rendus Méc. 342 (5), 334–346.
Zhong, Y., He, S., Ji, B., 2012. Mechanics in mechanosensitivity of cell adhesion and its roles in cell migration. Int. J. Comput. Mater. Sci. Eng. 1 (4), 1250032.
Zhong, Y., Ji, B., 2013. Impact of cell shape on cell migration behavior on elastic substrate. Biofabrication 5 (1), 015011.
Zhong, Y., Ji, B., 2014. How do cells produce and regulate the driving force in the process of migration? Eur. Phys. J. Spec. Top. 223, 1373–1390.
Zhong, Y., Kong, D., Dai, L., Ji, B., 2011. Frequency-dependent focal adhesion instability and cell reorientation under cyclic substrate stretching. Cell. Mol. Bioeng. 4 (3), 442–456.